A Small-World Network Based Framework for Texture Classification

Shubham Dwivedi, Keerthika Kadagala, Om Jee Pandey*, and Rajesh M. Hegde
Indian Institute of Technology Kanpur, India, *Indian Institute of Technology (BHU), Varanasi, India.
Email: {shubhamd21, keerthika21, rhegde}@iitk.ac.in, *omjee.ece@iitbhu.ac.in

***Abstract*—Textures often exhibit both strong local patterns and long-range repetitions, which are important cues for classification. We propose a small-world network based method that models each image as a multi-scale patch graph. The graph starts as a regular lattice and is enriched with two types of long-range links: (i) similarity-guided links connecting distant but feature-similar patches, and (ii) Fourier-guided links that follow the dominant spatial frequency. The small-world role is twofold: (i) we construct small-world graphs by adding these informed links, and (ii) we extract features that capture small-world properties such as clustering and path length, along with mixing behavior and spectral structure. These features summarize the graph and help distinguish textures. The final feature vector, aggregated across scales, is then used with a classifier. Results on the Brodatz dataset show competitive performance compared to classical texture descriptors. Experiments also demonstrate that the proposed method is more robust to noise and rotation than existing approaches.**

***Index Terms*—Small-world networks, Texture classification, Complex networks, Graph signal processing, Fourier analysis**

I. Introduction

The problem of texture classification is a fundamental problem in computer vision that aims to recognize and classify surfaces based on their texture structure and statistical characteristics [1]. However, due to the ubiquitous presence of textures, having a reliable texture recognition system is essential in a number of application areas such as medical imaging [2], [3], industrial inspection [4], [5] and remote sensing [6]. One challenging aspect of this is the design of representations that are able to incorporate fine local regularities, as well as repeated or correlated patterns on longer spatial scales. Concurrently, these representations should be invariant with respect to changes of orientation, scale and noise. Requirements have inspired the evolution of techniques that are taking into account the structural relationships between the different parts of an image.

Over the years, several hand-crafted texture descriptors have been suggested. Global intensity or frequency distributions can be described with first order statistics and Fourier descriptors [7] but these do not provide a good description of local spatial organization. Multi-scale frequency representations are provided by gabor filter banks [8], [9] and wavelet transforms [10], [11], but are sensitive to rotation. While Gray-Level Co-occurrence Matrices (GLCM) [12] and Local Binary Patterns (LBP) [13], [14] are good for modeling the local spatial dependencies, they fail to capture long-range similarities between distant regions. Fractal [15]–[17] and lacunarity-based descriptors [18], [19] have been used in order to describe the self-similarity and scale-related behavior of textures, but they cannot always capture the complexity of real texture patterns.

To address these challenges, this work suggests a Small-World Network (SWN) based approach for texture classification [20]. SWNs are based on graph theory and feature a high degree of clustering at the local level and short average path lengths. This is done to allow local and global interactions, and hence information to flow efficiently throughout the network. This is commonly seen in natural and social systems, and has been found to enhance the robustness of complex networks and efficient communication between them [21]–[25]. These properties have motivated the proposed approach which represents each texture image as a multi-scale graph. The structure is built on a regular lattice of image patches, with two complementary forms of long-range connections added on: links between patches that are spatially far away but have a similar visual content; links based on the dominant spatial-frequency direction. By leveraging small-world properties, the proposed method captures both local and global structures in a unified framework, offering a powerful alternative.

II. Proposed Method

This section outlines the methodology in detail and describes the process of constructing the proposed framework. The proposed framework is illustrated in Figure 1.

A. Patches and Base Lattice

Let $\mathbf{I} \in \mathbb{R}^{H\times W}$ be a grayscale image. For each grid size $s \in \{8, 12, 16\}$ we crop $\mathbf{I}$ to multiples of s, partition the image into a regular $s \times s$ grid of non-overlapping patches of size

$$(b_h, b_w) = \big(\lfloor H/s \rfloor,\ \lfloor W/s \rfloor\big),$$

and index grid coordinates by $(i, j) \in \{0, \dots, s-1\}^2$ with node index $u = i\,s + j$. The number of nodes is $N = s^2$. For patch $\mathbf{P}_{ij}$ we compute a 13-dimensional descriptor

$$\phi_{ij} = \big[\mu,\ \sigma,\ H_{32},\ \bar{g},\ \sigma_g,\ \mathrm{OH}_1, \dots, \mathrm{OH}_8\big] \in \mathbb{R}^{13},$$

where μ, σ are the intensity mean and standard deviation; $H_{32} = -\sum_{b=1}^{32} p_b \log_2 p_b$ is the 32-bin entropy of intensities with p_b the normalized histogram; $\bar{g}, \sigma_g$ are the mean and standard deviation of the gradient magnitude computed with Sobel kernels

$$K_x = \begin{bmatrix} -1 & 0 & 1 \\ -2 & 0 & 2 \\ -1 & 0 & 1 \end{bmatrix}, \qquad K_y = \begin{bmatrix} -1 & -2 & -1 \\ 0 & 0 & 0 \\ 1 & 2 & 1 \end{bmatrix},$$

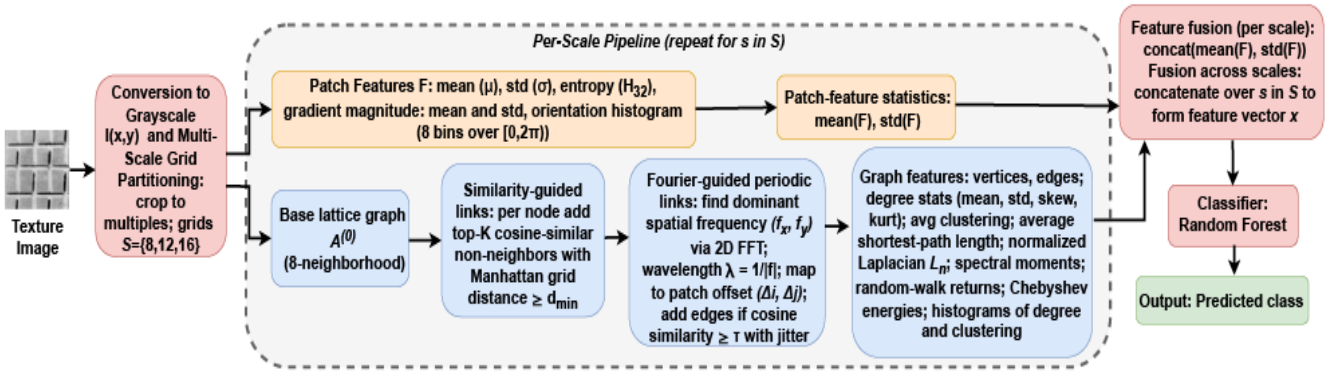

Fig. 1: Proposed small-world network based model: multi-scale patches form a base lattice enhanced with similarity and Fourier links, producing a small-world graph. Extracted structural and signal features are then classified for improved accuracy.

and OH_b is an 8-bin orientation histogram [26]weighted by gradient magnitude,

$$\mathrm{OH}_b = \frac{1}{\sum_{p\in\mathbf{P}_{ij}} \|\nabla\mathbf{I}(p)\|} \sum_{p\in\mathbf{P}_{ij}} \|\nabla\mathbf{I}(p)\|\, \mathbf{1}\{\theta(p)\in[\alpha_b,\alpha_{b+1})\}$$

with $\theta(p) = \operatorname{atan2}((\mathbf{I}*K_y)(p), (\mathbf{I}*K_x)(p))$, and $\{\alpha_b\}_{b=1}^{9}$ uniform over $[0, 2\pi)$. Stacking ϕ_{ij} row-wise yields $F \in \mathbb{R}^{N\times 13}$.

We create the base lattice by connecting each node to its 8-neighborhood on the grid including diagonals. Let $A^{(0)} \in \{0,1\}^{N\times N}$ be the symmetric adjacency with zero diagonal, and let $\mathcal{N}_8(i,j)$ denote the 8-neighbors of (i,j). Then

$$A^{(0)}_{uv} = 1 \quad \Leftrightarrow \quad (i_u, j_u) \in \mathcal{N}_8(i_v, j_v).$$

B. Addition of new links: Similarity and Fourier links

We enrich $A^{(0)}$ with two families of long-range links.

1) Similarity-guided links: Row-normalize F to unit ℓ_2 norm to obtain $\widehat{F}$ and compute cosine similarities [27]

$$S = \widehat{F}\,\widehat{F}^{\top} \in [-1,1]^{N\times N}.$$

Let the Manhattan grid distance be $\delta(u,v) = |i_u - i_v| + |j_u - j_v|$. For each node u we define the candidate set

$$\mathcal{C}_u = \{v \neq u :\ A^{(0)}_{uv} = 0,\ \delta(u,v) \geq d_{\min}\},$$

and select

$$\mathcal{E}_{\mathrm{sim}}(u) = \underset{v\in\mathcal{C}_u}{\arg\operatorname{topK}} S_{uv},$$

with $K = 3$ and $d_{\min} = 3$. We add undirected links (u,v) for all $v \in \mathcal{E}_{\mathrm{sim}}(u)$. This preserves local clustering from the lattice while reducing path lengths through semantically consistent shortcuts.

2) Fourier-guided periodic links: To capture near-periodicity, we estimate a dominant spatial frequency from a normalized grid signal of patch means. Let

$$M \in \mathbb{R}^{s\times s}, \qquad M_{ij} = \mu_{ij},$$

where μ_{ij} is the mean intensity of patch $\mathbf{P}_{ij}$. Let

$$\widetilde{M} = M - \frac{1}{s^2}\sum_{i,j} M_{ij}.$$

We compute the 2-D discrete Fourier transform $F_M = \mathcal{F}\{\widetilde{M}\}$ and its magnitude $P = |F_M|$, suppress the 3×3 DC neighborhood, and locate the maximum at index $(k^\star, \ell^\star)$. With frequency origin at the center (k_0, ℓ_0), the normalized frequencies are

$$f_x = \frac{\ell^\star - \ell_0}{s}, \qquad f_y = \frac{k^\star - k_0}{s}, \qquad f = \sqrt{f_x^2 + f_y^2}.$$

The dominant-frequency magnitude defines a displacement scale $\lambda = \frac{1}{f+\varepsilon}$, and the direction is $\theta = \operatorname{atan2}(f_y, f_x)$. In the implementation, this scale is projected along the dominant direction and normalized by the patch size (b_h, b_w) to obtain a patch-grid displacement:

$$\Delta i = \operatorname{round}\left(\frac{\lambda\sin\theta}{b_h}\right), \qquad \Delta j = \operatorname{round}\left(\frac{\lambda\cos\theta}{b_w}\right).$$

If $(\Delta i, \Delta j) = (0,0)$, we set $\Delta j = 1$. For each node at (i,j), candidate targets of the form

$$(i', j') = (i + \Delta i + \eta_i,\ j + \Delta j + \eta_j)$$

are considered, with integer jitter $\eta_i, \eta_j \in \{-1, 0, 1\}$. If (i', j') lies within the grid, the edge is added only when the cosine similarity S_{uv} between the corresponding nodes satisfies $S_{uv} \geq \tau$ with $\tau = 0.2$. Up to K_{four} Fourier-guided links may be added per node. Let $\mathcal{E}_{\mathrm{four}}$ denote the set of accepted links. The final adjacency at scale s is

$$A = A^{(0)} \ \vee\ A_{\mathrm{sim}} \ \vee\ A_{\mathrm{four}}.$$

C. Feature extraction, aggregation, and classification

Let $D = \operatorname{diag}(A\mathbf{1})$ and $L_n = I - D^{-1/2}AD^{-1/2}$ be the normalized Laplacian. Here, $\mathbf{1}$ denotes the all-ones vector in $\mathbb{R}^N$. We treat three per-patch attributes as graph signals aligned with the node order: the mean intensity μ, the entropy H_{32}, and the gradient-magnitude mean $\bar{g}$.

1) Topology features: From the adjacency matrix A, we compute the following features in a single vector: size features given by the node count N and edge count $m = \frac{1}{2}\mathbf{1}^{\top}A\mathbf{1}$; degree statistics where $k_u = \sum_v A_{uv}$ and we record the mean $\bar{k}$, standard deviation σ_k, skewness $\gamma_1 = \frac{1}{N}\sum_u \left(\frac{k_u - \bar{k}}{\sigma_k + \varepsilon}\right)^3$, and

kurtosis $\gamma_2 = \frac{1}{N}\sum_u \left(\frac{k_u-\overline{k}}{\sigma_k+\varepsilon}\right)^4$; the average local clustering coefficient $\overline{C}$ with $C_u = \frac{2T_u}{k_u(k_u-1)+\varepsilon}$ and $T_u = \frac{(A^3)_{uu}}{2}$; a landmark-based estimate of the average shortest-path length $\tilde{L}$ obtained via breadth-first search from a fixed set of evenly spaced landmarks and averaging finite distances; spectral moments $m_2 = \mathrm{tr}(L_n^2)$ and $m_3 = \mathrm{tr}(L_n^3)$ (with L_n the normalized Laplacian); and normalized histograms (10 bins each) of the degree distribution and of the set $\{C_u\}$.

2) Random-walk returns and Chebyshev graph-signal energies: With transition matrix $P = D^{-1}A$, the return probabilities

$$\rho_k = \frac{1}{N}\,\mathrm{tr}\big(P^k\big), \qquad k = 1, \ldots, 4,$$

summarize the mixing behavior induced by hubs, cycles, and long-range links. Define $L_d = L_n - I$. For a signal $o \in \mathbb{R}^N$ we compute Chebyshev polynomials by

$$T_0(o) = o, \;\; T_1(o) = L_d o, \;\; T_k(o) = 2L_d T_{k-1}(o) - T_{k-2}(o),$$

and record energies $E_k(o) = \|T_k(o)\|_2$ for $k = 0, 1, 2, 3$ and $o \in \{\mu, H_{32}, \bar{g}\}$. These energies probe increasingly nonlocal filtering on the graph.

3) Per-scale descriptor and aggregation: At each scale s we concatenate: topology features, $\{\rho_k\}_{k=1}^4$, the Chebyshev energies for the three signals, the degree histogram, the clustering histogram, and global patch statistics given by the feature-wise mean and standard deviation over the rows of F. Concatenating the per-scale vectors for $s \in \{8, 12, 16\}$ yields the final descriptor $x \in \mathbb{R}^d$.

4) Classification: The descriptor x is given to a classifier. We use a random forest with 100 trees. Other choices can also be used without modifying the graph construction. The predicted label is $\hat{y} = \mathcal{C}(x)$ with $\mathcal{C} : \mathbb{R}^d \to \{1, \ldots, C\}$.

III. PERFORMANCE EVALUATION

A. Experimental setup

1) Dataset: We used the Brodatz texture dataset, a standard benchmark for texture classification tasks. The dataset consists of 111 grayscale texture classes, each represented by a single image of size 640×640 pixels. To increase the number of training samples, each image was divided into 25 non-overlapping patches of size 128×128 pixels. This resulted in a total of 2775 texture images. The dataset was split into training and testing sets using an 80:20 ratio with class-stratified sampling.

2) Training details: Training and testing were conducted on a system equipped with an Intel(R) Xeon(R) Silver 4214R CPU @ 2.40GHz. All extracted features were standardized using z-score normalization. A Random Forest classifier with 100 estimators was used for classification. The overall accuracy, along with class-wise evaluation parameters, was used to assess the performance of the model. All methods were evaluated with the same preprocessing pipeline and hyperparameter settings to ensure a fair comparison.

B. Experimental results

1) Accuracy analysis: The proposed method was compared to some of the well known texture classification approaches such as first order statistics, Fourier descriptors, Gabor filters, wavelet transforms, Haralick features, Local Binary Patterns (LBP), and various lacunarity/fractal-based descriptors. As shown in Table 1, the proposed method also performed the best with noise-free data, and had an accuracy of 92.97% compared to all of the other competing approaches. The first order statistics presented only 69.19% accuracy, as they were only able to describe the intensity distribution at a single point. The Fourier descriptors gave 79.82% and the discrete cosine transform gave 85.59%. These techniques obtain frequency-related information, but they are not spatially localized in representation so they are not discriminative. The results on Wavelet feature showed an accuracy of 82.88%, which achieved an improvement in accuracy by performing multi-scale analysis, but had lower accuracy for complex texture variations. The results were remarkably good for Haralick and LBP, with an accuracy of 87.21% and 86.31%, respectively. They are, however, local to the pixel-relationship and parameter selections and thus not robust to geometric variations. Of the traditional methods, the Gabor filters gave the best result with an accuracy of 91.71%, capturing the multi-scale and multi-orientation responses. However, the accuracy obtained by the proposed method was still higher. Fractal and lacunarity based methods, showed a weaker performance and the results were not as good. The accuracy of the Bouligand–Minkowski descriptors was 51.89% and the accuracy of the mass–radius descriptors was 63.96%, while the accuracy of the lacunarity based descriptors was between 69.19% and 75.32%. The results indicate that such descriptors are not as effective to capture the discriminative information of the structure. The combination of multi-scale grid partitioning and graph based feature extraction is responsible for the superior performance of the proposed method, as it allows the encoding of local texture characteristics and higher-order spatial dependencies.

2) Noise and Rotation Analysis: Noise and rotation analysis are performed on the image. All methods were tested with additive Gaussian noise with a variance of $\sigma^2 = 0.1, 1, 2$ and under rotations of the images of $45°, 90°, 135°$ to further assess their robustness. As can be seen from Table 1, a significant degradation was observed for many of the traditional descriptors in the noisy environment. First-order statistics and differential lacunarity accuracy fell below 10% at $\sigma^2 = 2$ and the Haralick and LBP features also significantly reduced their accuracy, due to the need of precise local pixel arrangements. Fourier and DCT descriptors were relatively more noise tolerant, but in the more severe noise cases, at $\sigma^2 = 2$ both of them were less discriminative, giving only 12.61% and 20.36% accuracy, respectively. Wavelet features were moderately robust with 31.35% accuracy at $\sigma^2 = 1$ but their accuracy also decreased with the variance of the noise level. Although the Gabor filters were less sensitive to noise than most other traditional descriptors, with 80.90%

TABLE I: Performance comparison of the proposed model with existing techniques under additive Gaussian noise ($\sigma^2 \in \{0, 0.1, 1, 2\}$) and rotation transformations ($45°$, $90°$, $135°$).

Method	**Accuracy (%)**						
	σ^2				**Rotation**		
	0	0.1	1	2	$45°$	$90°$	$135°$
First-order statistics	69.19	28.29	10.09	6.49	59.10	69.19	59.28
Fourier descriptors [7]	79.82	73.15	24.14	12.61	82.52	79.82	81.26
Gabor filter bank [9]	91.71	80.90	48.47	24.86	89.91	91.89	89.55
Wavelet (DWT) [10], [11]	82.88	62.52	31.35	18.92	69.19	81.08	68.83
Haralick (GLCM) [12]	87.21	63.24	15.14	7.57	83.78	87.57	83.42
DCT [28]	85.59	72.43	35.50	20.36	78.20	86.31	77.66
GLDM [29]	86.31	72.79	26.67	14.59	85.59	85.95	85.77
LBP [13]	86.31	55.14	14.59	9.19	82.16	85.41	81.44
Lacunarity (global) [18]	75.14	69.73	41.26	32.43	78.20	75.14	78.38
Lacunarity (local) [18]	75.32	48.47	37.12	29.55	78.38	75.32	77.48
Differential lacunarity [19]	74.77	28.83	4.32	1.44	69.19	74.77	69.37
Lacunarity 3D [18]	69.19	49.91	37.12	25.77	67.39	69.19	67.39
Fractal (Bouligand–Minkowski) [15]	51.89	30.81	2.16	1.80	56.04	51.89	55.32
Fractal (average square difference) [16]	68.29	65.05	35.14	22.70	74.05	67.93	74.95
Fractal (mass–radius) [17]	63.96	49.31	16.22	8.47	62.70	64.68	64.86
Proposed Method	**92.97**	**82.16**	**35.50**	**23.42**	**89.91**	**92.79**	**90.45**

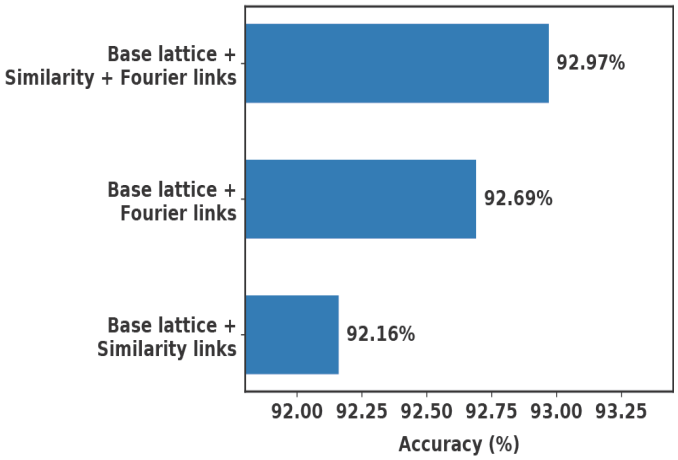

Fig. 2: Accuracy comparison of different configurations.

accuracy at $\sigma^2 = 0.1$, there was still some degradation in the highest noise levels. The proposed approach showed more stable results with accuracy of 82.16%, 35.50%, 23.42% for $\sigma^2 = 0.1, 1, 2$ respectively. In terms of rotation, the proposed method achieved accuracies of 89.91%, 92.79%, and 90.45% at $45°$, $90°$, and $135°$, demonstrating strong rotation invariance. Competing approaches such as Haralick features, LBP, and wavelet descriptors showed noticeable sensitivity to orientation changes, with accuracies dropping below 84% for rotated textures. Fourier and DCT descriptors retained better performance under rotation due to their global frequency representations, while Gabor filters maintained high rotation robustness comparable to our method. Overall, the proposed approach demonstrates both highly competitive baseline accuracy and resilience to noise and geometric transformations, owing to its ability to jointly exploit multi-scale local features and global graph-based structural information.

3) Effect of Similarity-Guided and Fourier-Guided Links: An ablation study was conducted to evaluate the individual and joint contributions of similarity-guided and Fourier-guided links within the proposed graph construction framework. As shown in Fig. 2, when combined with the base lattice, Fourier-guided links achieved an accuracy of 92.69%, whereas similarity-guided links achieved 92.16%. This suggests that Fourier-guided connectivity is more effective in capturing discriminative texture characteristics, indicating that periodic structural cues play an important role in the representation. The best performance was obtained when both similarity-guided and Fourier-guided links were incorporated together, resulting in an accuracy of 92.97%. This improvement that the two link construction mechanisms capture complementary aspects of texture structure.

4) Effect of Link Density on Accuracy: An ablation study was conducted for the grid size 8 configuration to examine the effect of graph connectivity by varying the total number of links. The low, medium, and high settings produced average actual total link counts of 584.84, 645.71, and 706.62, with corresponding classification accuracies of 91.53%, 92.85%, and 92.43%, respectively. The results show that accuracy improves as the number of links increases from the low to the medium setting, but declines slightly when the graph is further densified in the high setting. This behavior suggests that increasing connectivity is beneficial only up to an optimal level, beyond which additional links do not provide further gains and may slightly reduce the discriminative capacity of the resulting graph representation.

5) Analysis of Small-World Characteristics: The small-worldness measure, SW_N [30], characterizes the topology of a graph by comparing its clustering coefficient (CC) [24] and average path length (APL) [24] with those of an equivalent random graph R. It is expressed as:

$$SW_N = \frac{CC_N/CC_R}{APL_N/APL_R} = \frac{\Gamma}{\Lambda} \tag{1}$$

where Γ and Λ represent the normalized clustering coefficient and normalized average path length, respectively. A graph is considered to exhibit small-world behavior when $SW_N > 1$. We observed that after the addition of new links, the final graphs satisfied the criterion for small-world structure.

IV. CONCLUSION

In this paper, we proposed a novel Small-world network based approach for texture classification that integrates multi-scale grid partitioning with similarity and frequency-guided long-range connections. By leveraging both local statistical features and global spatial relationships through graph representations, the method effectively captures complex texture patterns across varying scales. Comprehensive experiments conducted on the Brodatz texture dataset demonstrated that the proposed method outperforms a wide range of traditional and state-of-the-art descriptors, achieving the highest classification accuracy under clean conditions. Furthermore, the method exhibited strong robustness to additive Gaussian noise and rotational transformations, consistently maintaining superior performance where other techniques degraded significantly. These results validate the effectiveness and generalizability of the proposed framework for real-world texture analysis tasks. Future work may explore extending the method to color textures, large-scale datasets, or integrating it with deep learning pipelines for hybrid representations.

ACKNOWLEDGEMENT

This work is supported by the ANRF-ARG under project number ANRF/ARG/2025/007629/ENS.

REFERENCES

[1] Manal Benzyane, Mourade Azrour, Imad Zeroual, and Said Agoujil, "State-of-the-art methods for dynamic texture classification: A comprehensive review," *Sustainable and Green Technologies for Water and Environmental Management*, pp. 1–13, 2024.

[2] Walid El-Shafai, Samy Abd El-Nabi, Anas M Ali, El-Sayed M El-Rabaie, and Fathi E Abd El-Samie, "Traditional and deep-learning-based denoising methods for medical images," *Multimedia Tools and Applications*, vol. 83, no. 17, pp. 52061–52088, 2024.

[3] Filip Orzan, Ştefania D Iancu, Laura Dioşan, and Zoltán Bálint, "Textural analysis and artificial intelligence as decision support tools in the diagnosis of multiple sclerosis–a systematic review," *Frontiers in Neuroscience*, vol. 18, pp. 1457420, 2025.

[4] Chuqiao Xu, Linchen Xu, Kai Luo, Jitao Zhang, Adilanmu Sitahong, Ming Yang, and Chengjun Zhang, "The essence and applications of machine vision inspection for textile industry: a review," *The Journal of The Textile Institute*, pp. 1–25, 2024.

[5] Qi Qiao, Huiying Hu, Azlin Ahmad, and Ke Wang, "A review of metal surface defect detection technologies in industrial applications," *IEEE Access*, 2025.

[6] Rashid N Mgohele, BHJ Massawe, Mawazo J Shitindi, Hilda G Sanga, and MM Omar, "Prediction of soil texture using remote sensing data. a systematic review," *Frontiers in Remote Sensing*, vol. 5, pp. 1461537, 2024.

[7] Robert Azencott, Jia-Ping Wang, and Laurent Younes, "Texture classification using windowed fourier filters," *IEEE Transactions on Pattern Analysis and Machine Intelligence*, vol. 19, no. 2, pp. 148–153, 1997.

[8] Saritha Suvarna and Demian Antony D'Mello, "A concise review of crop disease identification: Integrating conventional and deep learning feature extraction for effective diagnosis and mitigation strategies," in *International Conference on Inventive Communication and Computational Technologies*. Springer, 2024, pp. 93–106.

[9] Bangalore S Manjunath and Wei-Ying Ma, "Texture features for browsing and retrieval of image data," *IEEE Transactions on pattern analysis and machine intelligence*, vol. 18, no. 8, pp. 837–842, 2002.

[10] Tianhorng Chang and C-CJ Kuo, "Texture analysis and classification with tree-structured wavelet transform," *IEEE Transactions on image processing*, vol. 2, no. 4, pp. 429–441, 1993.

[11] Ingrid Daubechies, *Ten lectures on wavelets*, SIAM, 1992.

[12] Robert M Haralick, "Statistical and structural approaches to texture," *Proceedings of the IEEE*, vol. 67, no. 5, pp. 786–804, 1979.

[13] Timo Ojala, Matti Pietikainen, and Topi Maenpaa, "Multiresolution gray-scale and rotation invariant texture classification with local binary patterns," *IEEE Transactions on pattern analysis and machine intelligence*, vol. 24, no. 7, pp. 971–987, 2002.

[14] Yuyan Song, Jiming Sa, Yijie Luo, and Zhushanying Zhang, "A comprehensively improved local binary pattern framework for texture classification," *Multimedia Tools and Applications*, vol. 84, no. 20, pp. 22043–22068, 2025.

[15] André Ricardo Backes, "Upper and lower volumetric fractal descriptors for texture classification," *Pattern Recognition Letters*, vol. 92, pp. 9–16, 2017.

[16] Pedro García Sevilla, *Image processing: dealing with texture*, Wiley, 2006.

[17] Gabriel Landini and John W Rippin, "Notes on the implementation of the mass–radius method of fractal dimension estimation," *Bioinformatics*, vol. 9, no. 5, pp. 547–550, 1993.

[18] André Ricardo Backes, "A new approach to estimate lacunarity of texture images," *Pattern Recognition Letters*, vol. 34, no. 13, pp. 1455–1461, 2013.

[19] Pinliang Dong, "Test of a new lacunarity estimation method for image texture analysis," *International Journal of Remote Sensing*, vol. 21, no. 17, pp. 3369–3373, 2000.

[20] Shubham Dwivedi, Kartikeya Pandey, Kumar Shubham, Om Jee Pandey, Achyut Mani Tripathi, Tushar Sandhan, and Rajesh M Hegde, "Malanet: A small world inspired neural network for automated malaria diagnosis," *IEEE Transactions on Artificial Intelligence*, 2025.

[21] Shubham Dwivedi, Om Jee Pandey, and Rajesh M Hegde, "oswnn: Optimized small world neural network for predictive analysis," in *2025 National Conference on Communications (NCC)*. IEEE, 2025, pp. 1–6.

[22] Shubham Dwivedi, Tushar Sandhan, Om Jee Pandey, and Rajesh M Hegde, "swcnn: A small world convolutional neural network for efficient training," in *International Conference on Pattern Recognition*. Springer, 2024, pp. 359–374.

[23] Shubham Dwivedi, Tushar Sandhan, Om Jee Pandey, and Rajesh M Hegde, "Small-world inspired neural network (sw-nn) for an effective and accurate diagnosis of diabetes," in *2023 14th International Conference on Computing Communication and Networking Technologies (ICCCNT)*. IEEE, 2023, pp. 1–6.

[24] Shubham Dwivedi, Om Jee Pandey, and Rajesh M Hegde, "Swona: Small world inspired optimal neural architecture for smart neuropsychiatric diagnostics," *IEEE Transactions on Artificial Intelligence*, 2025.

[25] Shubham Dwivedi, Om Jee Pandey, and Rajesh M Hegde, "Aswe: Adaptive small-world encoder for efficient channel coding," in *ICASSP 2026-2026 IEEE International Conference on Acoustics, Speech and Signal Processing (ICASSP)*. IEEE, 2026, pp. 21401–21405.

[26] Hao Lu, Cunyu Sheng, and Wei Jia, "Palmprint recognition method based on orientation features: A survey," in *Chinese Conference on Biometric Recognition*. Springer, 2024, pp. 164–173.

[27] Sangwoo Park, Donggoo Kang, and Joonki Paik, "Cosine similarity-guided knowledge distillation for robust object detectors," *Scientific reports*, vol. 14, no. 1, pp. 18888, 2024.

[28] Isaac Ng, Tele Tan, and Josef Kittler, "On local linear transform and gabor filter representation of texture," in *Proceedings., 11th IAPR International Conference on Pattern Recognition. Vol. III. Conference C: Image, Speech and Signal Analysis,*. IEEE, 1992, pp. 627–631.

[29] Joan S Weszka, Charles R Dyer, and Azriel Rosenfeld, "A comparative study of texture measures for terrain classification," *IEEE transactions on Systems, Man, and Cybernetics*, , no. 4, pp. 269–285, 2010.

[30] Mark D Humphries and Kevin Gurney, "Network 'small-world-ness': a quantitative method for determining canonical network equivalence," *PloS one*, vol. 3, no. 4, pp. e0002051, 2008.